Available online at www.sciencedirect.com
ScienceDirect
Journal of Power Sources 162 (2006) 426–435
JOURNAL OF POWER SOURCES
www.elsevier.com/locate/jpowsour

# A three-dimensional PEM fuel cell model with consistent treatment of water transport in MEA

Hua Meng *

*Center for Engineering and Scientific Computation, College of Computer Science, P.O. Box 1455, Zhejiang University, Hangzhou, Zhejiang 310027, PR China*

Received 25 May 2006; received in revised form 13 July 2006; accepted 13 July 2006
Available online 23 August 2006

**Abstract**

In this paper, a three-dimensional PEM fuel cell model with a consistent water transport treatment in the membrane electrode assembly (MEA) has been developed. In this new PEM fuel cell model, the conservation equation of the water concentration is solved in the gas channels, gas diffusion layers, and catalyst layers while a conservation equation of the water content is established in the membrane. These two equations are connected using a set of internal boundary conditions based on the thermodynamic phase equilibrium and flux equality at the interface of the membrane and the catalyst layer. The existing fictitious water concentration treatment, which assumes thermodynamic phase equilibrium between the water content in the membrane phase and the water concentration, is applied in the two catalyst layers to consider water transport in the membrane phase. Since all the other conservation equations are still developed and solved in the single-domain framework without resort to interfacial boundary conditions, the present new PEM fuel cell model is termed as a mixed-domain method. Results from this mixed-domain approach have been compared extensively with those from the single-domain method, showing good accuracy in terms of not only cell performances and current distributions but also water content variations in the membrane.


*Keywords:* PEM fuel cell; Mixed-domain method; Interfacial boundary condition; Net water transfer coefficient; Water content

## 1. Introduction

Many multi-dimensional PEM fuel cell models have been developed in the past decade to facilitate cell design and optimization. These models generally fall into two categories: multi-domain and single-domain method. The studies of Gurau et al. [1] and Berning et al. [2] were based on the multi-domain method, in which the computational domain was divided into a number of sub-domains and different sets of conservation equations were developed in different sub-domains. Interfacial boundary conditions were further established to connect these equations. In the single-domain method, one set of conservation equations was applied to different regions of a PEM fuel cell. In order to switch on/off a specific equation in a specific region, special numerical treatments have been used, including defining extremely large or small physical and transport parameters in the region, i.e. very small proton conductivity outside the membrane electrode assembly (MEA). The studies of Um et al. [3], Dutta et al. [4], Siegel et al. [5], and Mazumder and Cole [6] were in this category.

Since there is only one set of conservation equations and no interfacial boundary condition, the single-domain method is easier to formulate and implement into a general CFD package. Recently, this method has experienced rapid development. For example, it has been applied to study electron transport phenomena [7,8], heat transfer [9], large-scale simulations [10–12], and two-phase flows and dynamics [13,14]. Extensive model validations have also been conducted [15,16].

A weakness of the single-domain method lies in its inability to handle water transport through the membrane phase directly, as theoretically the water content has to be solved in the membrane phase in MEA while the water concentration has to be solved in the other regions. In the study of Dutta et al. [4], the MEA region was completely neglected from the computational domain. As such, a simplified treatment was applied for water transport in the membrane phase. In the work of Um et al. [3], a fictitious

* Tel.: +86 571 87953166; fax: +86 571 87953167.
*E-mail address:* menghua@zju.edu.cn.

0378-7753/$ – see front matter © 2006 Elsevier B.V. All rights reserved.
doi:10.1016/j.jpowsour.2006.07.022

**Nomenclature**

| | |
|---|---|
| $a$ | water activity |
| $c$ | molar concentration (mol m$^{-3}$) |
| $C_p$ | constant-pressure heat capacity (J (kg K)$^{-1}$) |
| $D$ | mass diffusivity (m$^2$ s$^{-1}$) |
| $D_\lambda$ | water content diffusivity (mol (m s)$^{-1}$) |
| EW | equivalent weight of the membrane (kg mol$^{-1}$) |
| $F$ | Faraday constant (96487 C mol$^{-1}$) |
| $i$ | current density vector (A M$^{-2}$) |
| $I_{avg}$ | average current density (A m$^{-2}$) |
| $k$ | thermal conductivity (W (m K)$^{-1}$) |
| $n_d$ | electro-osmotic drag coefficient |
| $N_w$ | net water flux through the membrane (mol (m$^2$ s)$^{-1}$) |
| $p$ | pressure (Pa) |
| $q$ | interfacial flux |
| $R_u$ | universal gas constant (J (mol K)$^{-1}$) |
| $S$ | source term |
| $T$ | temperature (K) |
| $u$ | velocity (m s$^{-1}$) |

*Greek symbols*

| | |
|---|---|
| $\alpha$ | net water transfer coefficient |
| $\varepsilon$ | porosity |
| $\varepsilon_m$ | fraction of the membrane phase in the catalyst layer |
| $\phi$ | phase potential (V) |
| $\kappa$ | proton conductivity (S m$^{-1}$) |
| $\lambda$ | water content |
| $\mu$ | chemical potential |
| $\rho$ | density (kg m$^{-3}$) |
| $\sigma$ | electronic conductivity (S m$^{-1}$) |
| $\tau$ | viscous stress tensor |

*Supercripts*

| | |
|---|---|
| cl | catalyst layer |
| eff | effective value |
| m | membrane |

*Subscripts*

| | |
|---|---|
| cl | catalyst layer |
| e | electrolyte or energy |
| g | gaseous phase |
| $i$ | species |
| m | membrane |
| s | electron |
| sat | saturation value |
| w | water |

water concentration was derived to replace the variable of water content and therefore a same form of water transport equation could be solved in a single-domain framework [17]. The same treatment has also been proposed by Kulikovsky [18], but it was applied only in the two catalyst layers. Since in this treatment, the water content in the membrane phase was assumed to be in the thermodynamic equilibrium with the water concentration in every location, including inside the membrane, it seems that it is more appropriate to apply this treatment only in the catalyst layers, as the membrane phase is pervasively distributed and in extensive contact with water in these two regions [18]. It lacks theoretical basis to apply this method inside the membrane and this treatment is thus an approximation in this region. However, this treatment has been widely used in the studies of Meng and Wang [7,8,10], Ju et al. [9], and Wang and Wang [12,19], and it has been successfully validated by Ju and Wang [15] and Ju et al. [16] in terms of cell performances and current distributions. In the study of Siegel et al. [5], an extra transport equation for the dissolved water concentration was established in MEA, and a source term in the form of convective mass transfer was used to account for the water dissolution rate into the membrane phase. However, no expression has been presented for calculating this parameter. It is not clear how water transport through the membrane was handled in the study of Mazumder and Cole [6].

In this paper, a three-dimensional PEM fuel cell model with a consistent water transport treatment in the membrane electrode assembly has been developed. The concept of the fictitious water concentration is applied in the two catalyst layers. An extra conservation equation of the water content is solved in the membrane. Unlike Kulikovsky [18], however, a different set of internal boundary conditions at the interface of the membrane and the catalyst layer has been established, extending the one-dimensional formulation of Springer et al. [20] into the present three-dimensional framework. Since all the other conservation equations are still developed and solved in the single-domain paradigm, the present PEM fuel cell model is termed as a mixed-domain approach. In this paper, results from this mixed-domain approach have been compared to those from the single-domain method in detail.

## 2. Theoretical formulation

The conservation equations of mass, momentum, species concentration, proton, electron, and energy are still formulated exactly in the same forms as in the single-domain framework. They are in the following forms:

Mass:

$$\nabla \cdot (\rho \vec{u}) = 0 \tag{1}$$

Momentum:

$$\frac{1}{\varepsilon^2} \nabla \cdot (\rho \vec{u} \vec{u}) = -\nabla p + \nabla \cdot \tau + S_u \tag{2}$$

Species:

$$\nabla \cdot (\vec{u} c_i) = \nabla \cdot (D_i^{eff} \nabla c_i) + S_i \tag{3}$$

Proton transport:

$$\nabla \cdot (\kappa^{eff} \nabla \phi_e) + S_e = 0 \tag{4}$$

Electron transport:

$$\nabla \cdot (\sigma^{eff} \nabla \phi_s) + S_s = 0 \tag{5}$$

Energy:

$$\nabla \cdot (\rho C_p \vec{u} T) = \nabla \cdot (k^{\text{eff}} \nabla T) + S_T \tag{6}$$

In these equations, the source terms and the other relevant physicochemical parameters are presented in Meng and Wang [7,10] and Ju et al. [9].

Among the species concentration equations, the equation of the hydrogen concentration is solved only on the anode side while the equation of the oxygen concentration on the cathode side. In the present mixed-domain method, the equation of the water concentration is solved only in the gas channels, gas diffusion layers (GDL), and catalyst layers on both anode and cathode sides. Furthermore, in the two catalyst layers, the fictitious water concentration has been included to take into account of water transport in the membrane phase [17,18]. The effective water diffusion coefficient in the two catalyst layers can be expressed as

$$D_w^{\text{cl,eff}} = \varepsilon_{\text{cl}}^{1.5} D_w^{\text{cl,g}} + \varepsilon_m^{1.5} D_\lambda \frac{R_u T}{p_{\text{sat}}} \frac{d\lambda}{da} \tag{7}$$

More details can be found in Um and Wang [17] and Kulikovsky [18].

Unlike the prior single-domain method, a conservation equation of the water content is solved in the membrane in this mixed-domain method. The conservation equation is derived as follows:

$$\nabla \cdot (D_\lambda \nabla \lambda) + S_\lambda = 0 \tag{8}$$

where the source term arising from the electro-osmotic drag can be expressed as

$$S_\lambda = -\nabla \cdot \left( \frac{n_d \vec{i}}{F} \right) \tag{9}$$

In Eq. (8), because the fluid velocity is very small inside the membrane, the convective effect has been neglected.

As in the prior studies of Meng and Wang [7,8,10] and Um and Wang [17], the water content diffusivity in Eqs. (7) and (8) can be estimated as

$$D_\lambda = \frac{\rho_m}{\text{EW}} D_w^m = \frac{\rho_m}{\text{EW}} \times \begin{cases} 3.1 \times 10^{-7} \lambda (e^{0.28\lambda} - 1) \cdot e^{[-2346/T]} & 0 < \lambda \le 3 \\ 4.17 \times 10^{-8} \lambda (1 + 161 e^{-\lambda}) \cdot e^{[-2346/T]} & \text{otherwise} \end{cases} \tag{10}$$

Its variation is shown in Fig. 1.

The conservation equation of the water content, Eq. (8), is connected to the water concentration equation by a set of internal boundary conditions at the two interfaces between the membrane and the catalyst layers on both anode and cathode sides. As shown in Fig. 2, the interfacial boundary conditions can be established based on the thermodynamic phase equilibrium and the flux equality. The general thermodynamic phase equilibrium conditions at the interfaces are [21]

$$T^m = T^{\text{cl}} \tag{11a}$$

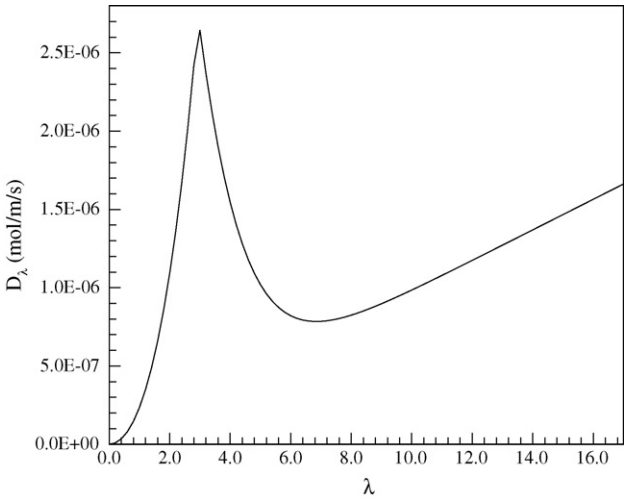


Fig. 1. Variation of water content diffusivity in the membrane phase.

$$p^m = p^{\text{cl}} \tag{11b}$$

$$\mu_w^m = \mu_w^{\text{cl}} \tag{11c}$$

The general flux equality conditions include the equal energy and water fluxes at the interface

$$\vec{q}_e^m = \vec{q}_e^{\text{cl}} \tag{12a}$$

$$\vec{q}_w^m = \vec{q}_w^{\text{cl}} \tag{12b}$$

Since the single-domain method is used for solving the energy equation, Eqs. (11a) and (12a) will be closely approached but are not explicitly required. Eq. (11b) is required for solving water transport in the membrane once liquid water is involved, as suggested in Weber and Newman [22]. In the present model development and the following numerical calculations, we will

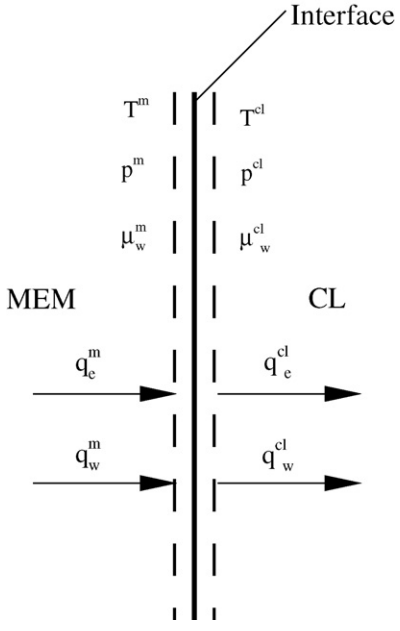


Fig. 2. Schematic of an interface and the interfacial boundary conditions.

only consider the pseudo single-phase cases, and therefore, this equation can be neglected.

According to Springer et al. [20], Eq. (11c) can be approximately replaced using the following empirical expression:

$$\lambda = \begin{cases} 0.043 + 17.18a - 39.85a^2 + 36.0a^3 & 0 < a \leq 1 \\ 14 + 1.4(a-1) & 1 < a \leq 3 \end{cases} \quad (13)$$

where the parameter λ represents the water content on the membrane side of the interface and the parameter $a$ is the water activity on the catalyst layer side of the interface.

The water flux equality at the interface can be further derived as

$$\left(-D_\lambda \nabla\lambda + \frac{n_d \vec{i}}{F}\right)\Big|_m = \left(-D_w^{cl,eff}\nabla C_w + \frac{n_d \vec{i}}{F}\right)\Big|_{cl} \quad (14)$$

Eqs. (13) and (14) constitute a set of the interfacial boundary conditions for connecting the two conservation equations of the water content in the membrane and the water concentration in the other regions.

The above conservation equations, Eqs. (1)–(6) and (8), and the set of interfacial boundary conditions, Eqs. (13) and (14), complete the model development in the present mixed-domain

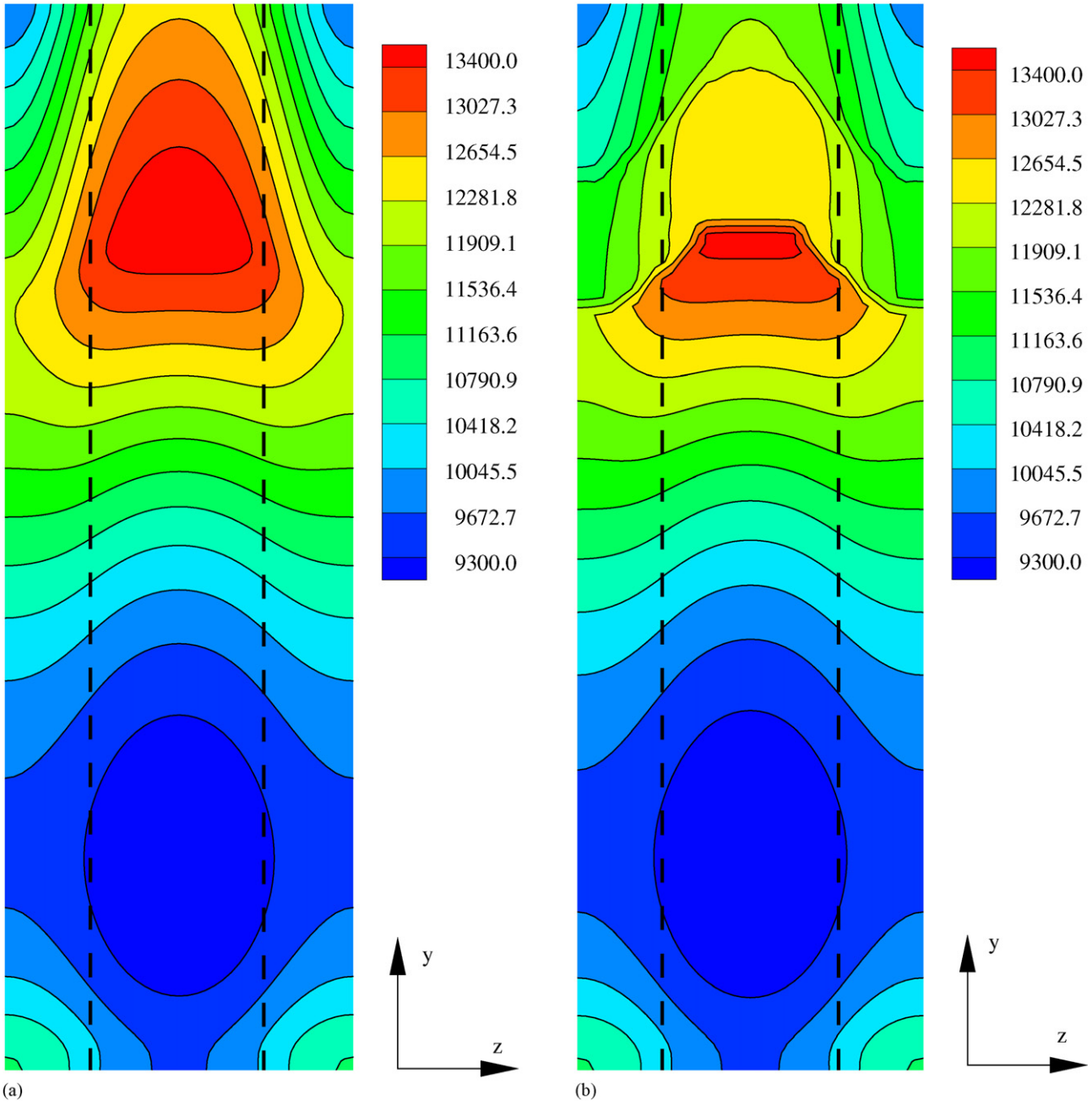


Fig. 3. Current distribution in the mid-thickness of the membrane: (a) from the mixed domain method, (b) from the single-domain method (unit: A $m^{-2}$).

method. The other relevant physicochemical relationships, boundary conditions, and numerical treatments follow the same procedures as in the single-domain approach, as detailed in Refs. [3,7,10]. This numerical model has been implemented into a general CFD package, Fluent. The computational grid used in the present study is the same as in the previous work [7,8], which is generated based on careful grid independence studies. In the next section, results from this mixed-domain approach will be compared with those from the single-domain method, which have been extensively validated in terms of cell performances and current distributions [15,16].

## 3. Result and discussion

The present numerical calculations are conducted using a single straight-channel PEM fuel cell with a thin membrane of 25 μm. Its geometry and the other related parameters are presented in Meng and Wang [7,8]. In the present configuration, the *x*-coordinate is in the through-membrane direction, *y*-coordinate the along-channel direction, *z*-coordinate the lateral direction. In order to make a comprehensive comparison, three different cases are designed for the present numerical study, as shown in Table 1. Since the cell operates at a constant temperature of 80 °C, two of the cases are in low-humidity operation conditions, consistent with the present pseudo single-phase calculations.

Table 1
Inlet humidification temperature and relative humidity at cell temperature of 80 °C

| Case number | Anode | | Cathode | |
|---|---|---|---|---|
| | Humidification temperature (°C) | Relative humidity (%) | Humidification temperature (°C) | Relative humidity (%) |
| Case 1 | 80 | 100 | 20 | 5 |
| Case 2 | 50 | 26 | 50 | 26 |
| Case 3 | 80 | 100 | 80 | 100 |

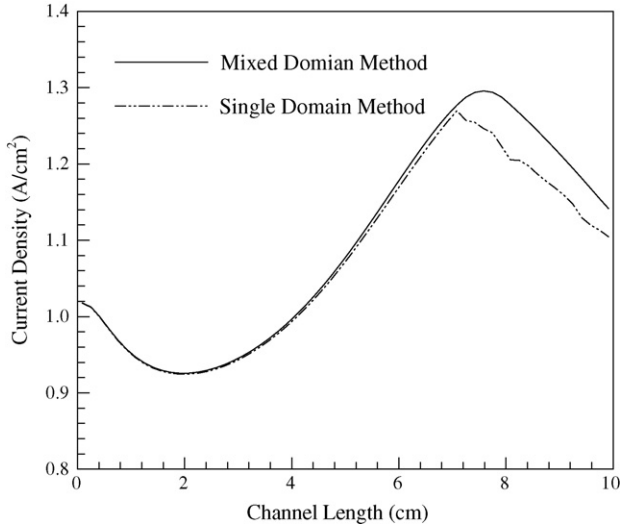


Fig. 4. Variation of average current density in the along-channel direction.

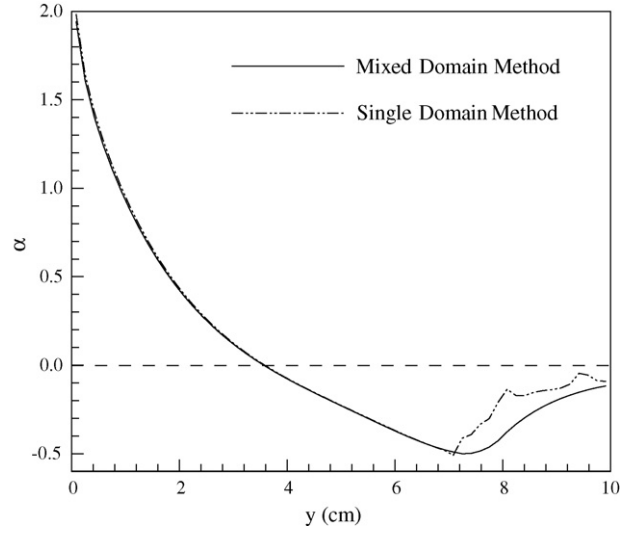


Fig. 5. Variation of the net water transfer coefficient in the along-channel direction.

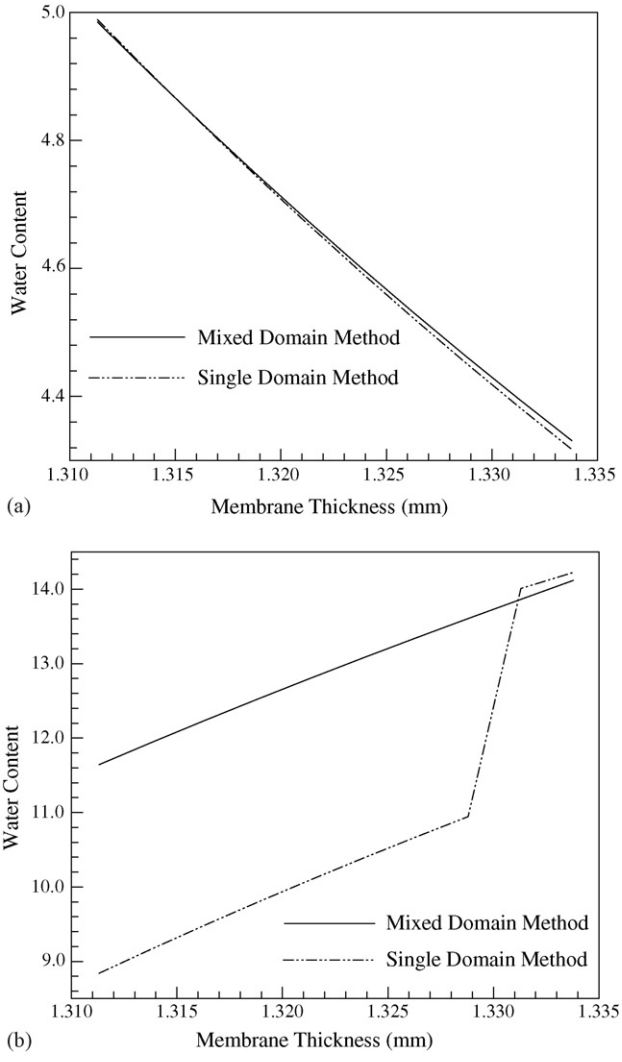


Fig. 6. Variation of water content inside the membrane under the gas channel: (a) at the inlet region, (b) at the outlet region.

The fully humidified case is included for completeness. The single-domain calculations are based on the model presented in Meng and Wang [7,10], which applies the fictitious water concentration concept in MEA [17]. In both the mixed-domain and the single-domain methods, the anisotropic electron transport phenomenon is handled using the simplified method developed in Meng [23], but the contact resistance is neglected.

Fig. 3 illustrates current distributions in the mid-thickness of the membrane from both the present mixed-domain and the single-domain methods for case 1. Results show an excellent agreement at the first two-third length of the cell from the cell inlet. The current distribution from the single-domain model shows irregular variation starting from the two-third cell length. The calculated current distribution from the present mixed-domain method gives smooth variation in the entire region. Variations of the average current density in the along-channel direction from the two methods are further compared in Fig. 4. The curves in Fig. 4 vary in the exactly same trend and show a very good agreement. In consistency with Fig. 3, the average current density from the single-domain method shows slight oscillations starting from the two-third cell length. The reason for the oscillations will be explained later in this section.

Fig. 5 presents variations of the amount of water transported through the membrane in terms of a net water transfer coefficient $\alpha$, which is defined as the ratio of the local net water transfer rate through the membrane and the average water production rate in the cathode catalyst layer

$$\alpha = \frac{2FN_{\mathrm{w}}}{I_{\mathrm{avg}}} \tag{15}$$

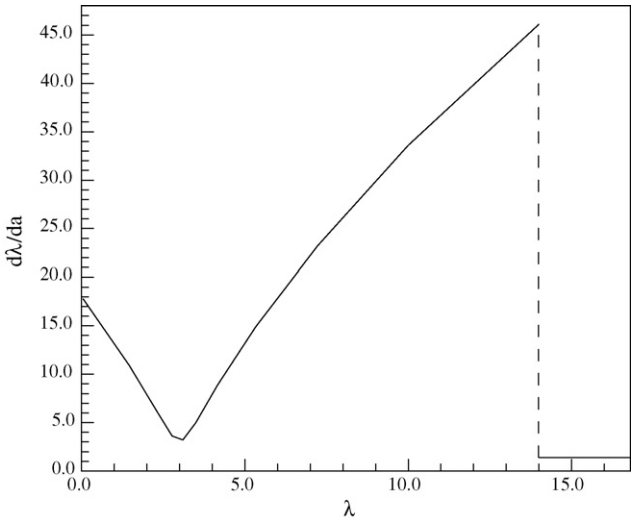


Fig. 7. Variation of the derivative term, $d\lambda/da$, with water content.

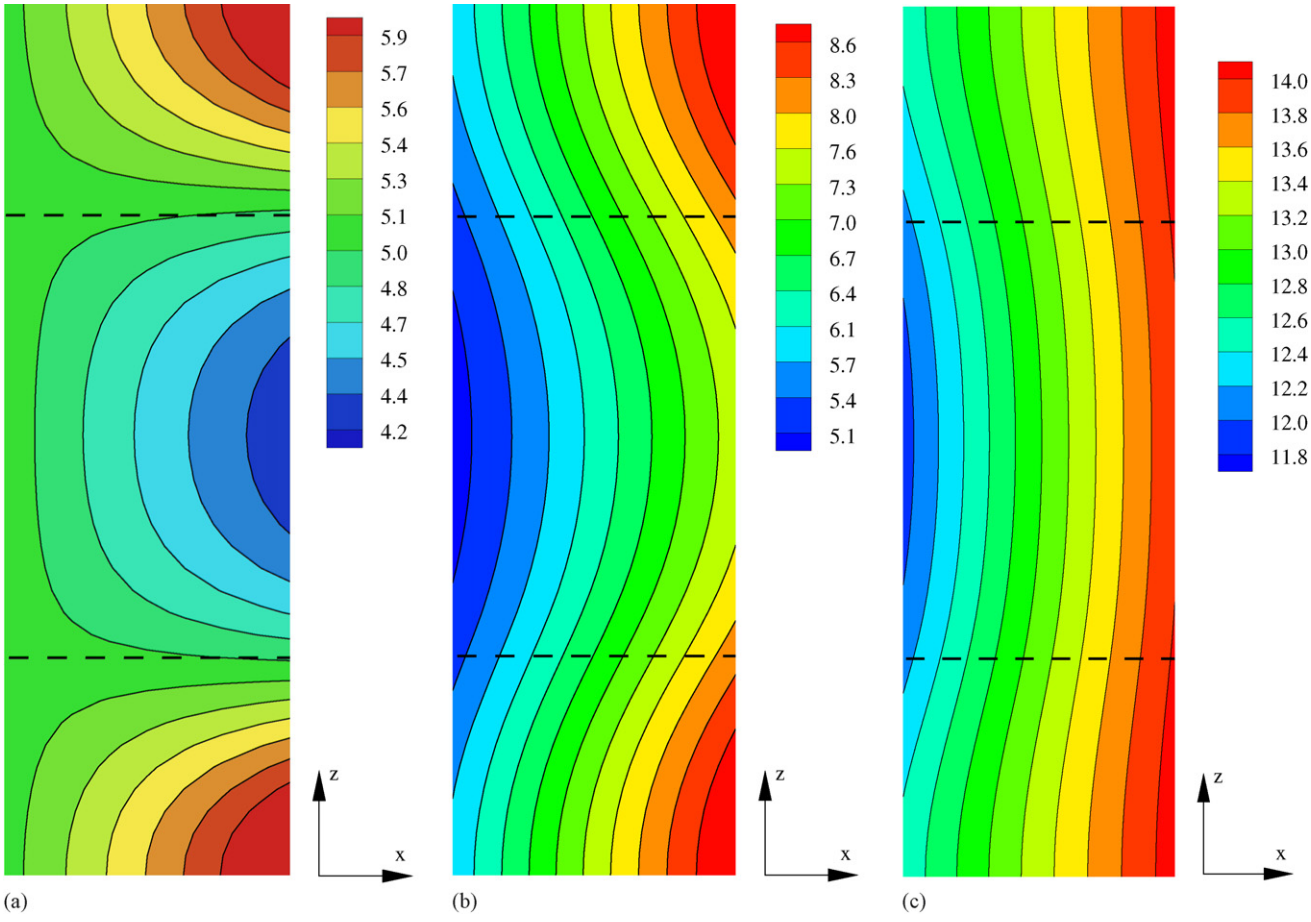


Fig. 8. Water content distribution in a cross section perpendicular to the membrane: (a) at the inlet region, (b) in the middle, (c) at the outlet region.

In Eq. (15), a positive value means that water is transferred from the anode to the cathode side. The net water transfer through the membrane is caused by two mechanisms in the present calculations, namely the electro-osmotic drag from the anode to the cathode side and water diffusion, whose direction depends on the gradient of the water concentrations on the two sides.

In Fig. 5, variations of the net water transfer coefficient calculated from the two methods are in an excellent agreement before the result from the single-domain method starts to oscillate. In both methods, the calculated net water transfer is from the anode to the cathode side at the beginning of the cell because of the dual effects of the higher water concentration on the anode side, which results in the forward water diffusion, and the electro-osmotic drag. At around $y = 4$ cm, the net water transfer coefficient changes to negative values. This is dictated by the backward water diffusion caused by the higher water concentration on the cathode side, which is produced by the electrochemical reaction.

Fig. 6 shows water content variations inside the membrane under the middle of the gas channel. In Fig. 6a close to the inlet region, the water content has higher values on the anode side, resulting in the forward water diffusion. Results from the two methods are in an excellent agreement. In Fig. 6b close to the outlet region of the cell, the water content shows higher values on the cathode side, resulting in the strong backward water diffusion. An interesting point is that although the curves show nearly the same gradient in the majority of the membrane, the result from the single-domain approach shows a sharp decrease at a water content value of $\lambda = 14$ close to the cathode side. This is not a physical phenomenon but a numerical result caused by the fictitious water concentration treatment, in which the water diffusivity involves a derivative term in the form of $d\lambda/da$. Fig. 7

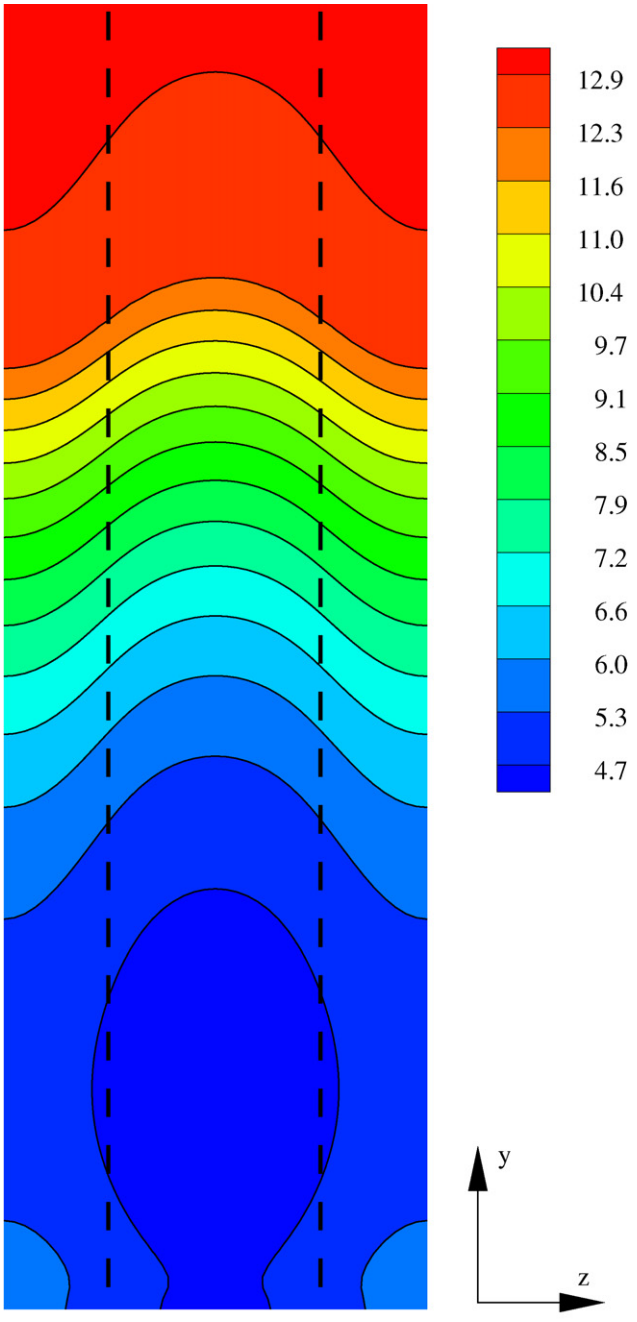


Fig. 9. Water content distribution in the mid-thickness of the membrane.

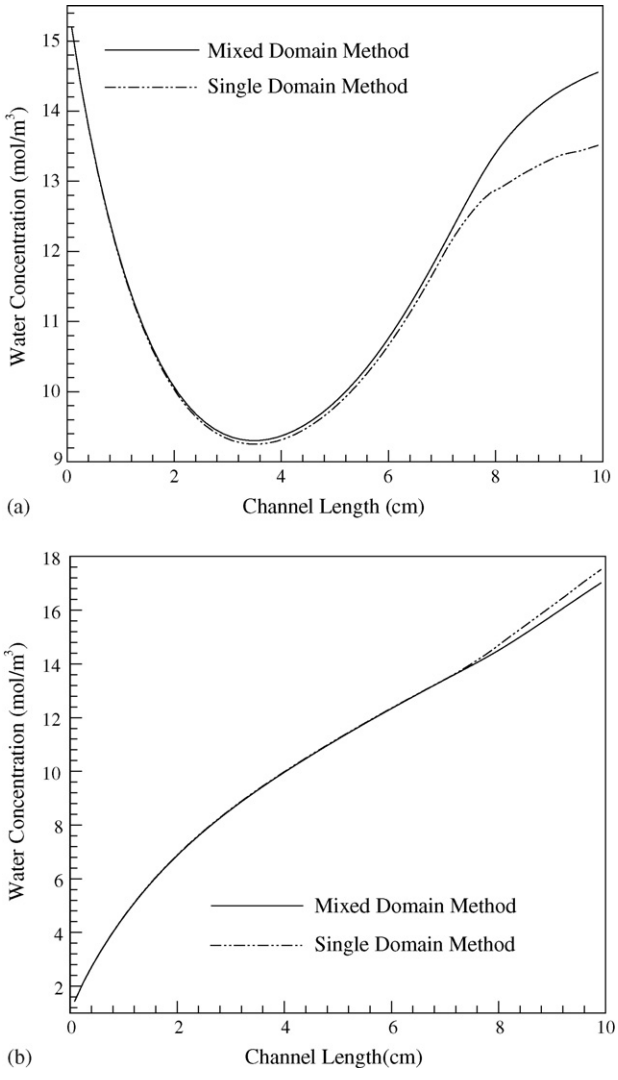


Fig. 10. Variation of water concentration in the gas channel: (a) on the anode side, (b) on the cathode side.

provides the variation of this derivative term calculated using Eq. (10). It shows an abrupt decrease at a water content of 14. This result indicates that the fictitious water concentration approximation could cause an incorrect water content variation inside the membrane. In fact, the sharp decrease of the water content in the single-domain approach, as shown in Fig. 6b, results in the lower water content values in the majority of the membrane, which in turn causes the lower water content diffusivity, as can be seen in Fig. 1, and consequently the higher net water transfer coefficient at the outlet region in Fig. 5. In addition, this incorrect water content variation also causes oscillations in the current distribution and the net water transfer coefficient in Figs. 3–5. It should be noted that in this case this type of problem only occurs under the fully humidified condition with a water activity above unity, i.e. close to the outlet region, but the incorrect water content variation could also occurs under low-humidification conditions, as discussed later in this section.

Water content distributions calculated from the present mixed-domain model are illustrated in Figs. 8 and 9. In Fig. 8, water content distributions are shown in three different cross sections perpendicular to the membrane. These results clearly show that the water content distribution in the membrane varies not only from the anode to the cathode side but also in the lateral direction, with the higher water content under the land than that under the channel. Fig. 8a illustrates that at the inlet region of the cell, although the water content is higher on the anode side under the gas channel, as also presented in Fig. 6a, it is higher on the cathode side under the land. Fig. 9 presents the water content distribution in the mid-thickness of the membrane, which clearly shows that the water content increases from the inlet to the outlet region, painting a complete picture of the water content variation inside the membrane.

Average water concentration variations in both the anode and the cathode gas channels from the two methods are presented in Fig. 10. Results from the two methods are in very good agreements as expected. Results are also consistent with the net water transfer coefficients presented in Fig. 5. For example, the water concentration in the anode gas channel initially decreases owing to the dual effects of the forward water diffusion and the

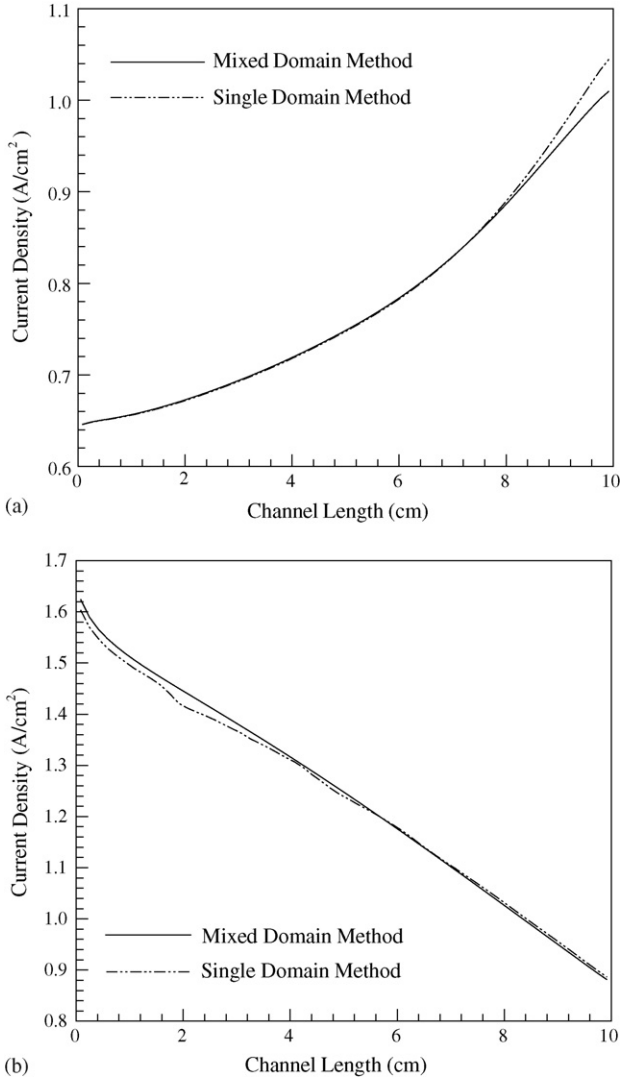


Fig. 11. Variation of the average current density in the along-channel direction: (a) from case 2, (b) from case 3.

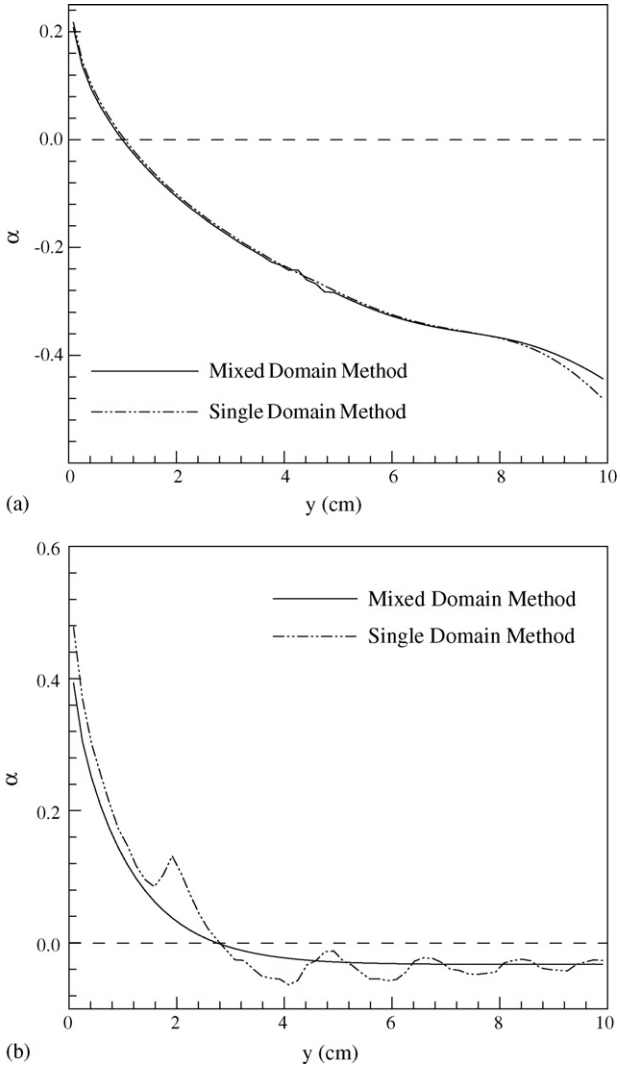


Fig. 12. Variation of the net water transfer coefficient: (a) from case 2, (b) from case 3.

electro-osmotic drag, and then increases dominated by the backward water diffusion. Furthermore, the differences from the two methods are consistent on the anode and the cathode sides as well.

Variations of the average current density from the mixed-domain and single-domain methods are further compared in Fig. 11, showing very good agreements for both cases 2 and 3. The net water transfer coefficient from the two methods is compared in Fig. 12. Results from case 2 in Fig. 12a show a very good agreement. Although results from case 3 in Fig. 12b are in the same trend, the result from the single-domain method shows large oscillations. These comparisons indicate that the single-domain method performs better under the low-humidification conditions than under the fully humidified ones, in consistency with the result from case 1. However, even under a low-humidification condition in case 2, the calculated water content in the membrane from the single-domain approach is different from the mixed-domain method, as shown in Fig. 13a at a location directly under the gas channel close to the outlet end. This can also be attributed to the approximate fictitious water concentration treatment in the membrane. Under the fully humidified condition in case 3, a rapid decrease of the water content calculated from the single-domain method again occurs inside the membrane, as shown in Fig. 13b.

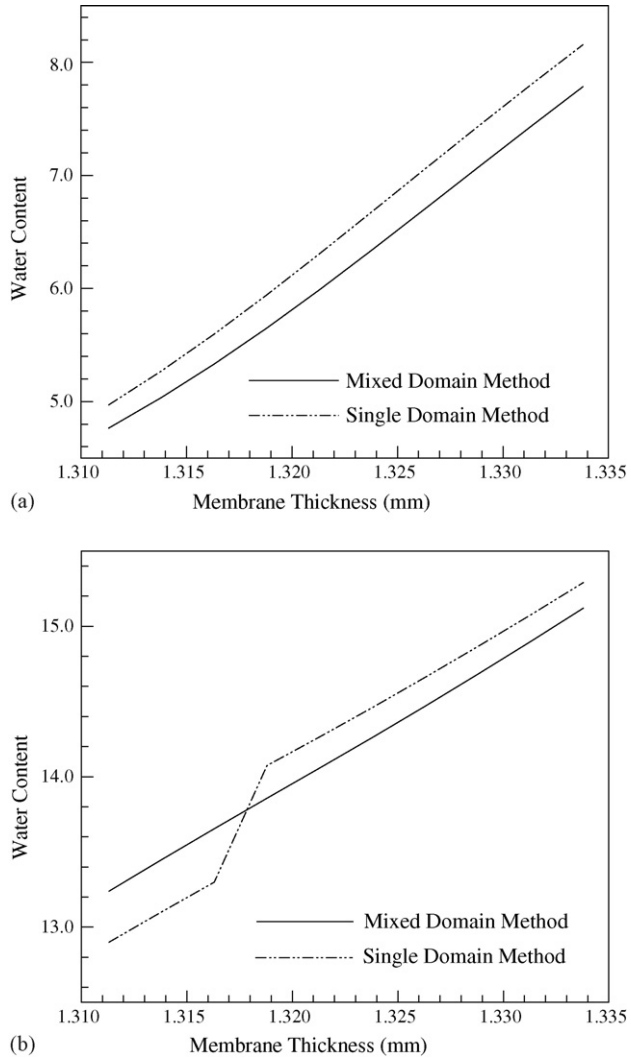


Fig. 13. Variation of water content inside the membrane under the gas channel at the outlet region: (a) from case 2, (b) from case 3.

Based on a comprehensive numerical analysis presented herein, it seems that the single-domain method using the fictitious water concentration approximation should be improved as it lacks theoretical basis inside the membrane and gives incorrect water content variations, although it can provide correct cell performances and current variations. The present mixed-domain method, which applies a set of interfacial boundary conditions to connect the conservation equation of the water content in the membrane and the water concentration equation in the other regions, is established on a solid theoretical basis and provides correct results in terms of not only cell performances and current variations but also water content variations inside the membrane. Furthermore, it seems that model validations based on cell performances and current variations are still insufficient since small differences in the current variation between the numerical and experimental data could indicate an incorrect result but it could easily escape a researcher's attention. It seems that the water content in the membrane and its related parameters, i.e. the membrane resistance, might have to be used for better model validation.

## 4. Conclusion

In this paper, a three-dimensional PEM fuel cell model with a consistent water transport treatment in the membrane electrode assembly has been developed. In this new PEM fuel cell model, the conservation equation of the water concentration is solved only in the gas channels, gas diffusion layers, and catalyst layers while a conservation equation of the water content is established in the membrane. These two equations are connected using a set of interfacial boundary conditions based on the thermodynamic phase equilibrium and flux equality at the interface of the membrane and the catalyst layer. In fact, this theoretical formulation extends the Springer's one-dimensional interfacial treatment into a three-dimensional framework. In addition, the prior fictitious water concentration treatment is applied in the two catalyst layers on a solid theoretical basis to consider water transport in the membrane phase. Since all the other conservation equations of mass, momentum, species concentration, proton and electron transport, and energy are still solved in the single-domain framework without resort to interfacial boundary conditions, the present new PEM fuel cell model is termed as a mixed-domain method. Results from this mixed-domain method have been compared extensively with those from the single-domain approach. The present model provides accurate numerical results in terms of not only cell performances and current variations but also water content variations inside the membrane.

## References

[1] V. Gurau, H. Liu, S. Kakac, Two-dimensional model for proton exchange membrane fuel cells, AICHE J. 44 (1998) 2410.

[2] T. Berning, D.M. Lu, N. Djilali, Three-dimensional computational analysis of transport phenomena in a PEM fuel cell, J. Power Sources 106 (2002) 284.
[3] S. Um, C.Y. Wang, K.S. Chen, Computational fluid dynamics modeling of proton exchange membrane fuel cells, J. Electrochem. Soc. 147 (2000) 4485.
[4] S. Dutta, S. Shimpalee, J.W. Van Zee, Three-dimensional numerical simulation of straight channel PEM fuel cells, J. Appl. Electrochem. 30 (2000) 135.
[5] N.P. Siegel, M.W. Ellis, D.J. Nelson, M.R. von Spakovsky, Single domain PEMFC model based on agglomerate catalyst geometry, J. Power Sources 115 (2003) 81.
[6] S. Mazumder, J.V. Cole, Rigorous 3-D mathematical modeling of PEM fuel cells. I. Model predictions without liquid water transport, J. Electrochem. Soc. 150 (2003) A1503.
[7] H. Meng, C.Y. Wang, Electron transport in PEFCs, J. Electrochem. Soc. 151 (2004) A358.
[8] H. Meng, C.Y. Wang, Multidimensional modeling of polymer electrolyte fuel cells under a current density boundary condition, Fuel Cells 5 (2005) 455.
[9] H. Ju, H. Meng, C.Y. Wang, A single-phase non-isothermal model for PEM fuel cells, Int. J. Heat Mass Transfer 48 (2005) 1303.
[10] H. Meng, C.Y. Wang, Large-scale simulation of polymer electrolyte fuel cells by parallel computing, Chem. Eng. Sci. 59 (2004) 3331.
[11] S. Shimpalee, S. Greenway, D. Spuckler, J.W. Van Zee, Predicting water and current distributions in a commercial-size PEMFC, J. Power Sources 135 (2004) 79.
[12] Y. Wang, C.Y. Wang, Ultra large-scale simulation of polymer electrolyte fuel cells, J. Power Sources 153 (2006) 130.
[13] S. Mazumder, J.V. Cole, Rigorous 3-D mathematical modeling of PEM fuel cells. II. Model predictions with liquid water transport, J. Electrochem. Soc. 150 (2003) A1510.
[14] H. Meng, C.Y. Wang, Model of two-phase flow and flooding dynamics in polymer electrolyte fuel cells, J. Electrochem. Soc. 152 (2005) A1733.
[15] H. Ju, C.Y. Wang, Experimental validation of a PEM fuel cell model by current distribution data, J. Electrochem. Soc. 151 (2004) A1954.
[16] H. Ju, C.Y. Wang, S. Cleghorn, U. Beuscher, Non-isothermal modeling of polymer electrolyte fuel cells. I. Experimental validation, J. Electrochem. Soc. 152 (2005) A1645.
[17] S. Um, C.Y. Wang, Computational study of water transport in proton exchange membrane fuel cells, J. Power Sources 156 (2006) 211.
[18] A.A. Kulikovsky, Quasi-3D modeling of water transport in polymer electrolyte fuel cells, J. Electrochem. Soc. 150 (2003) A1432.
[19] Y. Wang, C.Y. Wang, Modeling polymer electrolyte fuel cells with large density and velocity changes, J. Electrochem. Soc. 152 (2005) A445.
[20] T.E. Springer, T.A. Zawodzinski, S. Gottesfeld, Polymer electrolyte fuel cell model, J. Electrochem. Soc. 138 (1991) 2334.
[21] H.B. Callen, Thermodynamics and an Introduction to Thermostatistics, second ed., John Wiley & Sons, 1985.
[22] A.Z. Weber, J. Newman, Transport in polymer-electrolyte membranes. I. physical model, J. Electrochem. Soc. 150 (2003) A1008.
[23] H. Meng, A simplified method for solving anisotropic transport phenomena in PEM fuel cells, J. Power Sources 161 (2006) 466–469.